ORCA – Online Research @ Cardiff

Accelerated Molecular Dynamics to Explore Binding of Transition Metals to Amyloid-β

Oliver D. Kennedy-Britten, Nadiyah Alshammari, and James A. Platts*

School of Chemistry, Cardiff University, Park Place, Cardiff CF10 3AT, UK.

* Author for correspondence:

Email: platts@cardiff.ac.uk   Phone: +44-2920-874950

Abstract

We report accelerated molecular dynamics (aMD) simulation of amyloid-β (Aβ) peptides of four different lengths (16, 28, 40 & 42 residues) and their complexes when bound to Cu(II), Fe(II), or Zn(II). 600ns of equilibrated trajectory data was analysed for each structure from three independent 200ns aMD simulations, generating 16 aMD trajectories. We show that the presence of a metal ion leads to reduced size and decreased mobility relative to the free peptide, due to the anchoring effect of the ions. The reduced mobility was shown largely to be due to the restricted movement in N-terminal residues, most notably Asp1 and His6 that are involved in metal ion coordination in all cases. Significant disruption of secondary structure and patterns of salt bridge interactions arise on coordination of metal ions. In this regard, similarities were noted between results for Zn(II) and Fe(II), whereas results for Cu(II) are more comparable to the free peptides. Reweighting of free energy surfaces was carried out from aMD data to identify properties and descriptions of local minima structures.

Keywords Alzheimer's; Amyloid; Transition Metals; Molecular Dynamics; Free Energy; Secondary Structure

Introduction

One of the biggest challenges for medicine of the 21st century is developing understanding of aetiology and therapeutic methods for neurodegenerative diseases. The most common form of dementia is Alzheimer's disease (AD), an ailment the affects over two-thirds of dementia patients,[1,2] with estimated cases at over 1 million in the UK alone in 2021[3]. Pathological studies of AD patients show the presence of characteristic neuronal plaques consisting of soluble forms of the protein, amyloid-β (Aβ)[4,5]. These neurotoxic deposits, in conjunction with increased concentration of transition metals, are a distinguishing feature of [6,7]. It has been proposed that increased level of metal ions within the brain affect the homeostatic clearance and production rates of soluble Aβ species, leading to aggregation over a patient's lifetime[8,9]. This also explains the association of AD generally affecting elderly patients, aside from cases where genetic mutations are involved in early onset[10].

Aβ itself is a naturally occurring peptide, cleaved from the amyloid precursor protein (APP)[11,12] and found in all humans and other animals. So why isn't AD something that happens to us all as a standard part of aging? Since characteristic fibril structures were first identified by Alzheimer in a review from 1907[13] and subsequent investigations[14,15], the hypothesis on the role of Aβ a potential contributor to the causation of AD has developed and evolved. The amyloid cascade hypothesis originally considered concentration of Aβ alone[16] but there have been studies indicating the form Aβ takes is crucial, with soluble oligomers proving to be more toxic and harmful[17,18,19]. Heightened levels of transition metals in the brains of AD patients also affect rates of aggregation and solubility of Aβ, which can play a role in whether neurotoxic species are formed and to what degree[20,21]. A recent study used simulations to show that metal binding, particularly of Zn(II), increases the hydrophobicity of Aβ in its C-terminal region[22].

Full-length Aβ is 40 or 42 residues long (Figure 1), with the former more common but the latter having a higher proclivity to aggregate at levels associated with AD diagnosis[23,24,25]. Studies indicate that a higher incidence of β-strand secondary structure is potentially causative to protein misfolding and subsequent acceleration of aggregation[26,27,28,29]. Cu(II), Fe(II) and Zn(II) have high affinities for Aβ, binding to the N-terminus of the peptide (the first 16 residues)[30,31]. These metals can be found in varying abundance naturally, with Zn(II) being the most prevalent[32] of these ions found in senile plaques within the brain. The rate of

aggregation can be enhanced by these metals via production of reactive oxygen species (ROS) and formation of crosslinks between monomeric units of Aβ[33,34] which can further inhibit the clearance of an excess of the peptide. The variable oxidation states accessible to Cu and Fe may also play a role in ROS production.

N-terminus, metal binding region

DAEFRHDSGYEVHHQKLVFFAEDVGSNKGAIIGLMVGGVVIA

(1)　　　　　　(10)　　　　　(16)　　　(20)　　　　　　　　(28)　(30)　　　　　　　(40)　(42)

Figure 1- Amino acid sequence of Aβ42 highlighting N-terminus residues

In this work, we report accelerated molecular dynamics (aMD) simulations on metal bound Aβ peptides of varying lengths. aMD was selected for enhanced conformational sampling as well as being an appropriate method to simulate biomolecules of this size[35]. In addition, investigation via use of implicit solvent derived from the Generalised Born solvation model[36,37] allows better sampling and transitions between minima structures in comparison to conventional MD. Via the use of a boost potential from tailored parameters based on energy of the system under investigation, aMD overcomes energy barriers that would limit conversion between minima that may be inaccessible by conventional MD[38]. Subsequent analysis performed on equilibrated trajectories yield insight and comparative analysis into secondary structure, size, and intramolecular interactions.

Four chain lengths were selected; Aβ16 (to simulate effects solely within the metal binding region), Aβ40 & 42 (to examine properties of the full-length peptide and the aggregational properties of them mentioned previously), and Aβ28 (an intermediate length chain that has been used extensively experimentally and computationally[39,40,41,42]). For all four of these sequences, Cu(II), Fe(II), or Zn(II) were bound within the N-terminus. As well as these we modelled the free peptide with no metal centre. Thus, 16 structures were analysed in total.

Computational Methods

Four chain lengths (16, 28, 40, & 42 residues) of Aβ were manually constructed in extended conformations in MOE[43] in protonation states appropriate for physiological pH. All four

peptide lengths were modelled as both a free peptide as well as versions bound to copper, zinc or iron, creating sixteen structures in total. Cu(II) ions were coordinated via Asp1, His6 and His13; Zn(II) ions were bonded to Asp1, His6, Glu11 and His14; whereas Fe(II) were bound to Asp1, His6 and His14[44,45,46,47](Figure 2) . All structures were minimised with combination of AMBER94[48] and LFMM in DommiMOE[49], resulting in structures best characterised as random coil. From this point onwards, specific peptides with a metal centre will be referred to as Aβ[Chain Length]-Metal and any free peptides will be described as Aβ[Chain Length]-Free.
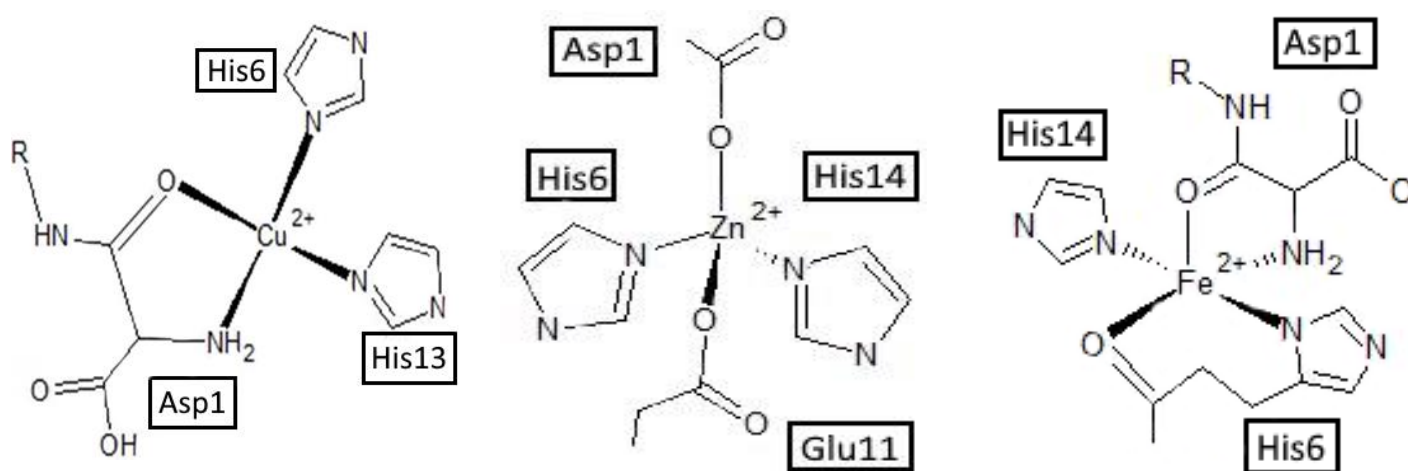

Figure 2- Binding modes of Aβ with Cu(II), Zn(II) and Fe(II)

All conventional and accelerated molecular dynamics (aMD) simulations were carried out using the AMBER16[50] package. Standard amino acids were modelled using the AMBER ff14SB[51] forcefield parameter set and the LEaP[52] module of AMBER, whereas parameters for metal-centres and any bound residues were generated via MCPB.py[53]. Bonded and non-bonded parameters for metal binding were extracted from B3LYP/6-31G(d) calculations performed using Gaussian09[54]. Harmonic bond length, angle and torsion parameters were extracted from the DFT Hessian using the Seminario[55] method, while non-bonded parameters were drawn from DFT electrostatic potential using the RESP method[54]. All simulations were performed in implicit solvent using the Generalised Born solvation model[56,57,58]. Previous work within our group shows comparable results between explicit and implicit solvent simulations on Aβ-Zn(II) structures, [59] with no improvement in results with explicit solvent. Implicit solvent is therefore used as it allows for more rapid simulations and conversion between conformations. Structures were first minimised by

1000 steps of steepest descent, followed by 1000 conjugate gradient steps. Implicit solvent has been shown to be a suitable solvent model for peptides of this nature without requirement for explicit solvent[60,61] and use of Generalised Born solvation model has been shown to enhance conformational sampling of mobile systems[62,63].

All simulations were performed in the NVT ensemble, in which temperature was regulated to remain at 310 K via use of a Langevin thermostat[64]. For all sixteen structures, three 50 ns conventional MD simulations were performed: each started from the same minimised starting structure but assigned a different set of random initial velocities sampled from the Maxwell-Boltzmann distribution. Subsequently, three independent 200 ns of aMD was performed, using the 16 final structures of each MD simulation as a starting point. Thus generating 48 individual simulations. Parameters for the boost potential in aMD were based on the size of the systems and the associated potential & dihedral energy from the prior MD calculations[65]. Calculations and values for the boost used in aMD calculations can be found in Supporting Information (Figure S1). From this, a bias potential was applied to boost the whole system simultaneously at points in the Potential Enegy Surface (PES) where the energy barrier would be too high to overcome using conventional MD[66].

The SHAKE algorithm[67] was implemented to ensure any bonds to hydrogens were maintained through the course of the simulation, and electrostatic interactions beyond 12 Å were disregarded. The initial 50 ns was removed to account for equilibration and the three 200 ns aMD data was combined for each structure (from the 48 aMD simulations in total) to form 600 ns trajectories for each of the individual sixteen systems. Analysis of these trajectories was carried out using CPPTRAJ v16.16[68] and VMD 1.9.3.[69] Free energy plots were constructed by re-weighting the boost potential from aMD following the procedures in refs [70,71].

Results and discussion

For all 16 structures, 50ns of cMD data was generated followed by 3 parallel 200ns aMD calculations. These aMD trajectories were then combined creating sixteen 600ns aMD trajectories, one for each structure. Each system has reached a quasi-equilibration point[72] during the initial 50 ns conventional MD for each run, as observed from RMSD data used as

a measure of equilibration. RMSD plots for individual simulations can be observed in figure S2. All data reported is taken from combined aMD data after this period of equilibration.

Radius of gyration (Rg) measurements were used as a measure of peptide size: Table 1 reports statistics for combined 600 ns aMD trajectories for (full graphs for individual trajectories in figure S3). Simulations for Aβ bound to zinc and iron generally showed the smallest average values suggesting these sampled more compact structures relative to the other simulations of comparable chain lengths. For 16 residue peptides, mean Rg is almost identical for free peptide and all three metals, but the maximum extent and standard deviation is lower when bound to metal, indicating that coordination to a metal centre within the N-terminus limits mobility and flexibility of these residues. For larger peptides, Zn and Fe binding restricts size and flexibility, as shown by relatively small maximum values, whereas Cu binding leads to similar or even greater size compared to free peptide. The increase in size and flexibility as the sequence is extended is also evident, although 40- and 42-residue peptides are not significantly different in mean or sd of Rg.

	Mean	Min	Max	sd
16				
Cu	7.78	6.59	9.94	0.41
Zn	7.72	6.94	8.86	0.24
Fe	7.94	7.19	9.40	0.26
Free	7.93	6.60	11.66	0.61
28				
Cu	10.53	8.23	15.63	1.44
Zn	9.69	8.16	14.27	0.96
Fe	10.35	8.24	14.78	1.19
Free	10.65	8.14	16.29	1.50
40				
Cu	11.49	9.19	21.36	1.72
Zn	10.95	9.07	19.05	1.40
Fe	11.48	9.16	20.37	1.56
Free	11.63	9.14	19.99	1.70
42				
Cu	12.38	9.29	21.35	2.07
Zn	10.86	9.20	20.37	1.22
Fe	11.46	9.26	19.08	1.50
Free	11.66	9.27	21.59	1.46

Table 1- Statistical analysis of radius of gyration (Rg) data (Å)

Similarities are evident in Rg statistics between zinc & iron-bound peptides and copper & metal-free structures, most notably in sd values, suggesting similar dynamics and

interactions within these two pairs of structures. Maximum Rg values for free peptides provide evidence of enhanced mobility as a result of an absence of a metal centre and highlight the potential for restriction in movement upon metal binding such as seen for zinc and iron containing structures. Rg data shows varying levels of mobility between simulations, with longer chain-lengths of Aβ-Cu and free Aβ showing relatively larger, more diffuse structures in comparison to peptides of the same length for zinc and iron.

Root mean square fluctuation (RMSF) data provides information on the level of mobility of individual residues within the simulations reported (Figure 3). Asp1 and His6 are coordinated to a metal-centre in all bound peptides. All free-peptide simulations have the highest RMSF values for these residues, demonstrating the anchoring effect of the metal centres within the N-terminus and the enhanced flexibility observed here in the absence of metal coordination. Values for metal binding residues in copper simulations are still relatively higher compared to other metal-bound structures. This could again provide further evidence of similarities in dynamics between these and free peptides. It could be suggested that binding of copper to Aβ provides less restriction on these structures as opposed to other metal centres giving rise to these enhanced RMSF values. Arg5 also gives some of the highest RMSF values in most Cu(II) simulations despite metal binding via the adjacent residue, His6. Binding of metal ions to Aβ peptides occurs within the N-terminus of all structures, yet results showed that effect of metal coordination on these molecules happened in both this region of the peptide as well as in residues remote to the coordination sites towards the C-terminus.

In the free peptides, the greatest contribution to flexibility shown arises from the Asp1 and His6 residues, which show largest increases in RMSF compared to all metal-bound peptides. The reported data indicating large peaks in mobility for residues towards the C-terminus for Fe(II)-bound structures confirms the effect of metal binding being a global effect on the peptide's structure as a whole as opposed to solely at the binding site. The mobility observed in the Rg data for Aβ40-Fe and Aβ42-Fe is also apparent from its RMSF data, most notably between residues Glu22-Lys28, which give the greatest contribution to the peptides' overall movement. This may be due to disruption of salt-bridges in this section of peptide induced by binding of Fe (*vide infra*).
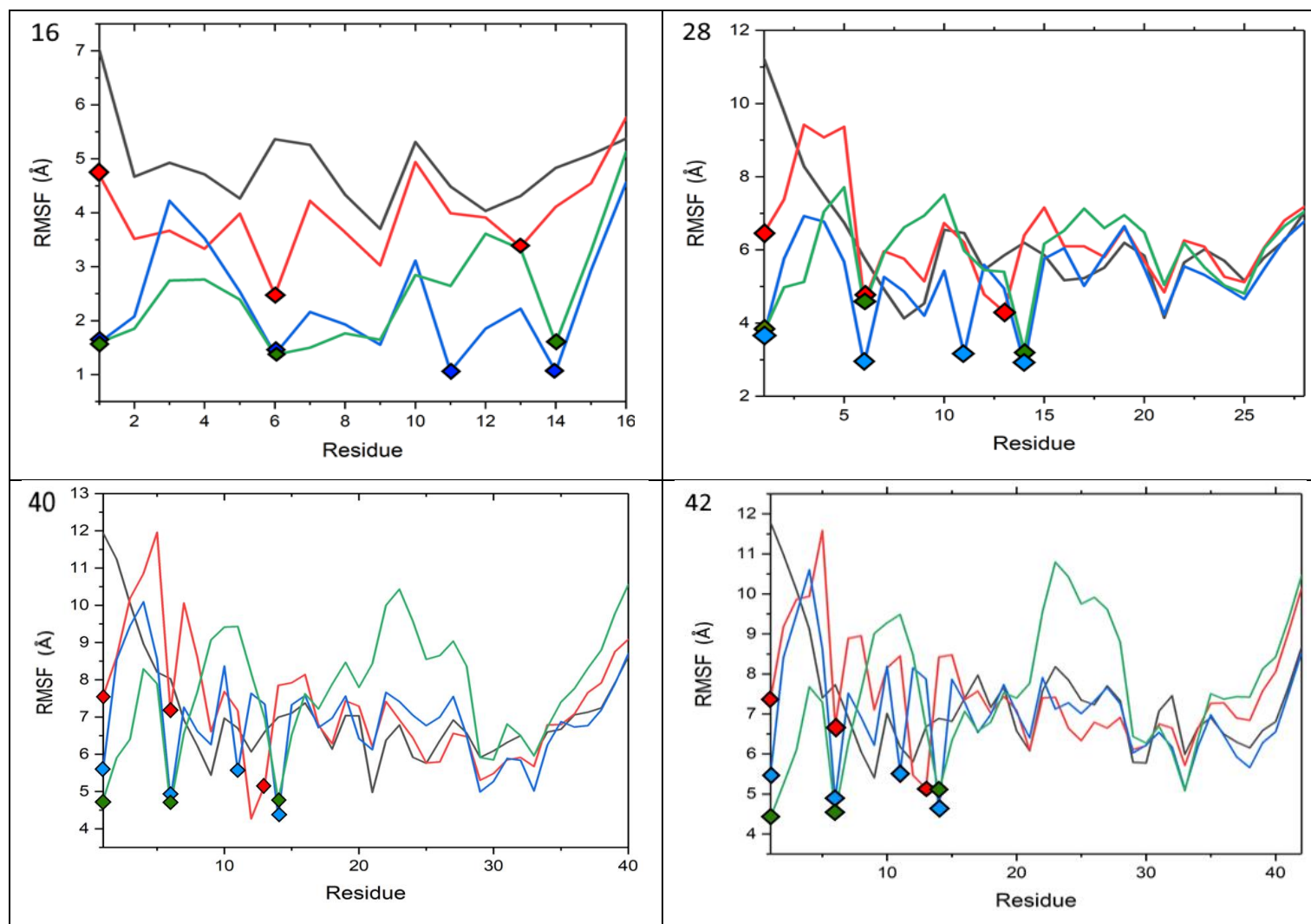
Figure 3- RMSF data (Å) based on individual residues. (Black = Free peptide, Red = Cu(II), Blue= Zn(II), Green = Fe(II) with bound residues highlighted in points of corresponding colours)

Cluster analysis identified and grouped sets of similar structures within a trajectory based on RMSD data of the peptide backbone via the DBSCAN[73] clustering algorithm within CPPTRAJ with a cut-off of 0.8 Å. The low amount of cluster data generated is evidence of our enhanced sampling of these highly flexible peptides. This shows some trajectories sampled such amounts of structures across the PES that they couldn't be categorised into similar conformational ensembles thus yielding low numbers or short-lived clusters. The simulations that did yield cluster data are highlighted in table 2 below. All simulations of 16 residue peptides are found to form some clusters: those for the free peptide and Aβ16-Cu

have rather low population, whereas for Aβ16-Zn and Aβ16-Fe over 70% of frames fall into just two clusters. Larger structures did not yield populated clusters: metal complexes of Aβ28 exhibit just 3 clusters with population of no more than 3%. A single cluster was found for Aβ42-Fe, but this was present for 0.9% of simulation time (approximately 540 frames out of 60,000).

Table 2- Cluster analysis data for equilibrated trajectories

Structure	# Clusters	Most populated (%)	2nd most populated (%)
Aβ16	6	8.8	1.6
Aβ16- Cu	36	11.9	5.2
Aβ16- Zn	12	51.8	21.8
Aβ16- Fe	7	61.9	10.7
Aβ28	0	-	-
Aβ28- Cu	3	0.7	0.7
Aβ28- Zn	3	1.3	0.5
Aβ28- Fe	3	2.8	0.5

Figure 4 displays the prevalence of salt-bridge contacts between charged residues for all trajectories by percentage of total frames (full percentage data for salt-bridge interactions can be found in Figure S4). Aβ16 has the lowest amount of potential salt-bridge combinations that can be formed due to the limited number of charged residues at the N-terminus. Types and occupation of salt-bridges formed in all four versions of the shortest peptide vary markedly, especially those involving Asp1 and Asp7 which are close to metal binding sites. Binding of Cu(II) reduces the number and persistence of
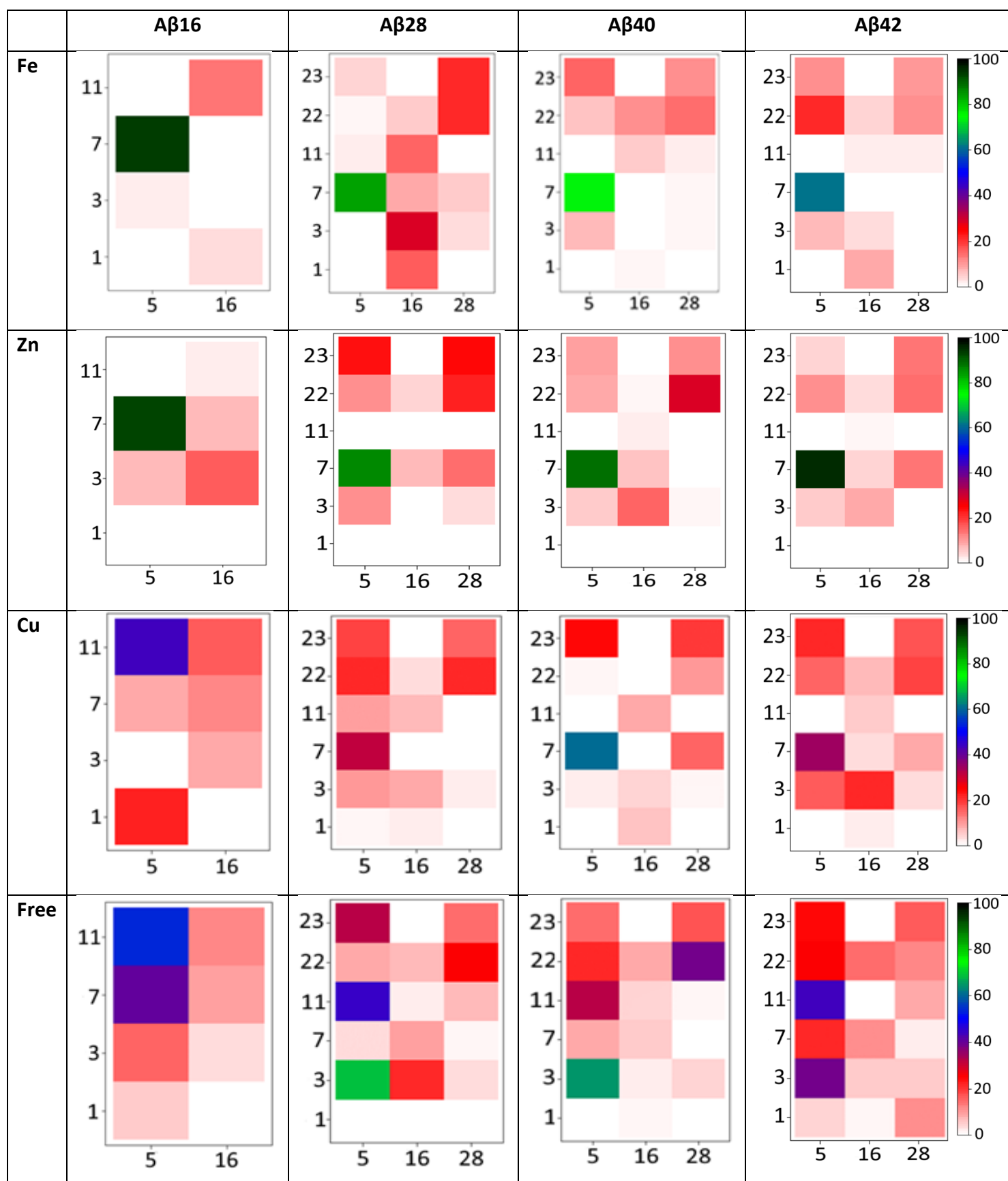
Figure 4- Salt bridge plots between charged residues by percentage incidence.

some more previously common interactions. In the shortest peptide, copper binding leads to almost complete loss of Arg5-Asp7, presumably due to metal binding at His6, while Arg5-Glu11 is common at similar incidence levels in both the copper-bound and free peptide. In Aβ16-Zn and Aβ16-Fe simulations however, percentage incidence of the interaction between Arg5-Asp7 increases notably whereas Arg5-Glu11 contacts are almost non-existent. The overall salt-bridge profile for these two structures is comparable in both types of interactions as well as frequency, further reinforcing the pattern noted above that Zn and Fe complexes behave similarly, while Cu complex shows behaviour closer to the free peptide. For example, Arg5-Asp7 maintains consistent incidence across all results for zinc and iron bound Aβ peptides, while copper and free peptide simulations show similarity.

The introduction of Glu22, Asp23 and Lys28 present several different combinations of potential salt-bridges that are not available in the shortest peptides. In the longer peptides, notable differences in salt-bridge formation are reported between the metallopeptide structures and the trajectories of those lacking in a metal centre. For instance, Arg5-Glu3 and Arg5-Glu11 contacts are common in longer metal-free peptides but almost completely absent in metal-bound systems. All interactions involving Lys28 occur at similar levels of incidence across all simulations where this residue is present. Interestingly, Lys16 and Asp23 appear to never be in contact in any trajectory. The most common salt-bridge interaction by percentage in all potential frames was between Arg5-Asp7, occurring at 55.5% of all simulation data.

Aβ is intrinsically disordered by nature yet secondary structure has commonly been associated with aggregational properties of Aβ. Misfolding of proteins and enhanced levels of β-sheet structures can give rise to increased propensity for formation of potentially neurotoxic species[74,75]. Incidence plots illustrate secondary structure type per residue across entire trajectories. These can be further classified as either helical, strand or other. Data for these plots can be found in Table 3. From the data reported here, levels of helical secondary structure in metal-bound structures increased as chain length of the peptide increased. The highest levels of secondary structure in all peptides are found as helices, which make up 30 to 40% of the larger peptides. This is particularly evident in Cu-bound and free peptide, for which almost all lengths of peptide adopt helical character for at least 30% of residues. For Zn and Fe complexes, helical content increases with peptide length but remains significantly

lower than Cu or free. Iron and Zinc simulations for 16-residue structures show considerably lower incidence levels of helix structure compared to all other data.

Table 3- Percentage of secondary structure types by residue classified as helical, strand, or other

	Fe			Zn			Cu			Free Peptide		
	Helix	Strand	Other	Helix	Strand	Other	Helix	Strand	Other	Helix	Strand	Other
AB16	1.1	< 0.1	98.8	2.2	1.2	96.6	30.0	1.1	68.9	22.1	1.7	76.2
AB28	18.6	0.2	81.2	24.8	1.1	74.1	29.5	0.5	70.0	45.0	0.8	54.2
AB40	23.3	1.4	75.3	25.8	1.9	72.3	31.5	1.1	67.4	42.4	1.2	56.4
AB42	28.3	0.8	70.9	30.7	1.7	67.6	33.8	1.4	64.8	38.1	3.4	58.5

For most simulations, the level of β-strand is slightly larger in the free peptide than in the metal-bound complexes, with the level broadly increasing in longer peptides. Aβ42-free shows the highest percentage incidence of β-strand at 3.4%, double the next most prevalent, namely Aβ16 and Aβ42-Zn at 1.7%. Beta strand secondary structure has commonly been associated with increased formation of neurotoxic species even at relatively low levels. The longest form of the peptide, Aβ42, has the greatest propensity for self-aggregation and in this experiment, Aβ42 free has the greatest value for levels of beta secondary structure which on the surface supports previous findings on the increased proclivity for aggregation possessed by this structure. However, it cannot be said with any certainty that the percentage incidence of strand/sheet secondary structure reported in Table 3 gives rise to the enhanced proclivity for aggregation into potentially neurotoxic species. A 2003 study conducted by Schmechel et al[76] showed levels of beta-sheet secondary structure at a higher incidence in comparison to those found from the simulation data presented here. This shows the levels of β-strand within the experimental results here do not replicate the levels of those observed in vivo to suggest increased Aβ toxicity[76].

Helical and strand secondary structure are generally absent or at very low levels within residues at the N-terminus for all metallopeptide simulations (Figure 5 for 42-residue peptides, with equivalent plots for others in Figure S5 in SI). All free peptide trajectories show an increase in the distribution of these forms of secondary structure across the whole peptide, mainly within residues towards the N-terminus mentioned previously. This further highlights the enhanced rigidity shown within this region due to coordination to a metal centre. As with the salt-bridge profiles, there is also a direct comparison that can be observed showing similarities in secondary structures levels and content between iron and zinc simulations as well as comparable data shown for copper-bound and free peptides.
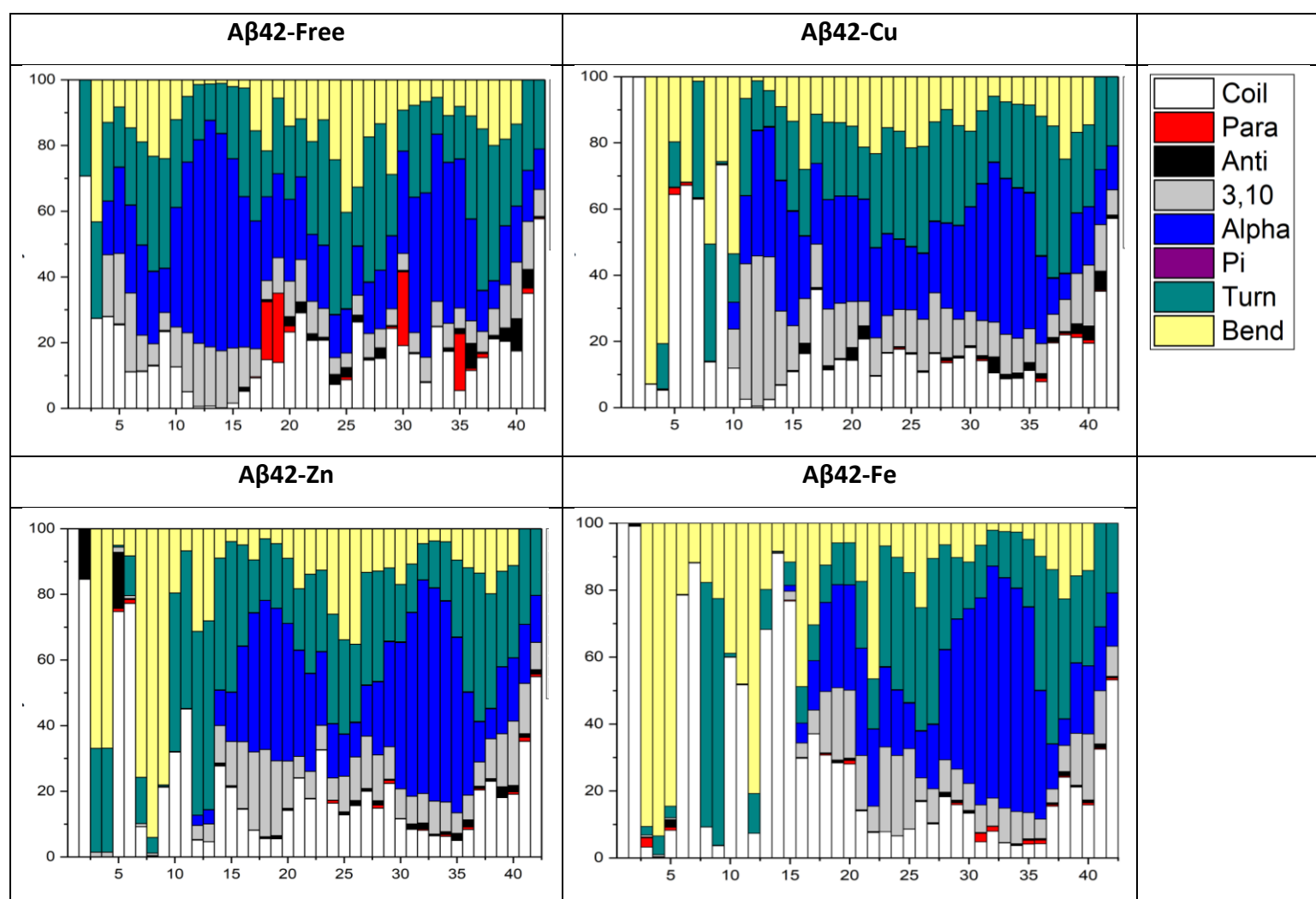

Figure 5- Secondary structure percentage incidence plots for Aβ42 simulations by residue

Secondary structure characterisation also demonstrates the effect of these ions within the metal-binding region of the N-terminus. There is a notable absence of any helical or strand

secondary structure within the first 10 residues of all metallopeptides analysed. They mainly arrange themselves into coil/turn/bend assemblies, and helical or strand secondary structures only form within this region when no metal centre is present. For all free peptides, organised secondary structure is present consistently throughout the whole peptide highlighting the relative rigidity caused by binding of a metal ion.

Hydrogen bond plots in Figure S6 illustrate interactions between appropriate atoms per residue based on their capacity as a donor or an acceptor. Statistics taken from these graphs, displayed in table 4, allow comparisons to be made on the formation of hydrogen bonds and thus the transient nature of conformations being sampled. As an implicit solvent is used in all simulations, any potential hydrogen bonding between peptides and solvents are not present in the model used.

Table 4- Statistical data for hydrogen bond plots of equilibrated aMD trajectories

	Mean	Min	Max	sd
16				
Cu	4.93	0	13	1.81
Zn	4.16	0	13	1.73
Fe	4.04	0	11	1.70
Free	6.46	0	16	2.04
28				
Cu	7.96	1	19	2.37
Zn	7.26	0	21	2.42
Fe	7.23	0	20	2.41
Free	9.38	0	22	2.81
40				
Cu	10.17	1	23	2.64
Zn	9.38	0	22	2.75
Fe	9.11	0	25	2.64
Free	11.07	1	24	3.00
42				
Cu	10.11	0	22	2.75
Zn	9.72	0	24	2.94
Fe	9.91	0	23	2.74
Free	12.10	1	27	3.15

Most simulations possess at least one structure with zero hydrogen bonds whilst maximum amounts of hydrogen bonds within simulations at given snapshots range from 13-27. This

shows the mobile nature of the peptides analysed, with folding and unfolding occurring over the course of the trajectories observed. Free peptides show the highest maximum, sd and average values indicating the particularly dynamic properties of Aβ in the absence of a metal centre. In comparison, zinc possessed the lowest average values of all types of structures analysed. This result was surprising as previously zinc structures were shown to have the lowest Rg values indicating it adopted potentially more compact conformations suggesting shorter contact distances between residues which would expect to encourage greater incidence of hydrogen bond interactions between residues. This suggests that potentially the structures were particularly transient which is supported by the increased number of different clusters in Aβ16-Zn, relatively lower RMSF values and short-lived salt-bridge contacts for example. Once again, similarities were observed in values between zinc and iron-containing systems supporting previous evidence of similarities in dynamics between Aβ peptides bound to these ions.

Taken together, the data recorded here reveal a picture of metal-induced disruption of peptide flexibility, secondary structure and salt-bridge patterns. While we have studied only monomers, some potential implications for aggregation can be drawn. The salt-bridge Asp23-Lys28 is known to play an important role in the kinetics of fibrillogenesis[77,78]: we find that this interaction is moderately populated in free and copper-bound peptides (16 to 19% of frames), but that this is significantly reduced in iron and zinc complexes. One can envisage, therefore, that metals might disrupt the β-turn structure required for the hydrophobic interactions that stabilise fibrils. Disruption of secondary structure is also evident; much of this is in the N-terminal region, that is not thought to play a role in aggregation[79]. However, we also see changes in regions such as the central hydrophobic cluster (L_{17}VFFA$_{21}$). In free Aβ42 especially, this sequence exhibits some β-strand character which is almost completely absent in all metal adducts. A similar effect is apparent in the hydrophobic residues in the C-terminal region, especially residues 35-40. Such β-strands have been proposed as a likely seed for aggregation[80], such that our results suggest metal ions may disrupt the canonical aggregation, perhaps leading to altered oligomers and aggregates and/or kinetics of association. Although these conclusions are highly speculative, it is clear that despite metal binding occurring exclusively in the N-terminal region, its

structural effects are felt across the whole peptide including those regions known affect aggregation.

Reweighting of the bias potential applied in accelerated MD recovers the free energy surface of the unbiased system, expressed as a function of properties of the system, known as potential of mean force (PMF). Plots of PMF as a function of Rg, hydrogen bond count, and end-to-end distance were used to examine energetic properties of structures sampled within the trajectories generated via aMD. PMF for Rg are plotted in Figure S7 in SI. Representative values of Rg were associated with minima structures for every trajectory. For the smaller peptides (16 & 28 residues long), the metal-free minima were found to possess a wider range of Rg within thermally accessible free energy, whilst Zn and Fe-bound peptides possessed the smallest range of Rg values for minima values for all simulations. For the larger chain lengths analysed (40 & 42 residues), the results for all trajectories were comparable to one another, occupying similar ranges of Rg between all trajectories.

Hydrogen bond count PMF plots showed that in general, peptides containing an iron or zinc metal centre possessed the lowest number and narrowest range of hydrogen bonds in low free energy structures. Free peptides generally exhibit more and wider range of hydrogen bonds, due to enhanced freedom of movement and interactions across the structure allowed by lack of hindrance that stems from coordination to a metal centre. Figure S8 shows these plots for all simulations as a representation of the trends observed across all structures.

Two-dimensional PMF employing Rg and end-to-end distance (from Asp1 to the final residue in the sequence) were plotted for all sixteen trajectories (Figure 6). Rg values for minima followed the same trend noted above of similar ranges between zinc & iron structures and copper and free peptides. Generally, across all peptide lengths, smaller ranges of Rg and end-to-end distance were observed within simulations for Aβ bound to iron and zinc compared to the other two sets of trajectory data. These lower values indicate that structures containing iron or zinc adopt more compact conformations and exhibit lower mobility as copper and free peptide, in accord with data from other results, as well as other experimental data for similar structures[81].

Figure 6- 2D plots of end-to-end distance against RoG as a function of free energy
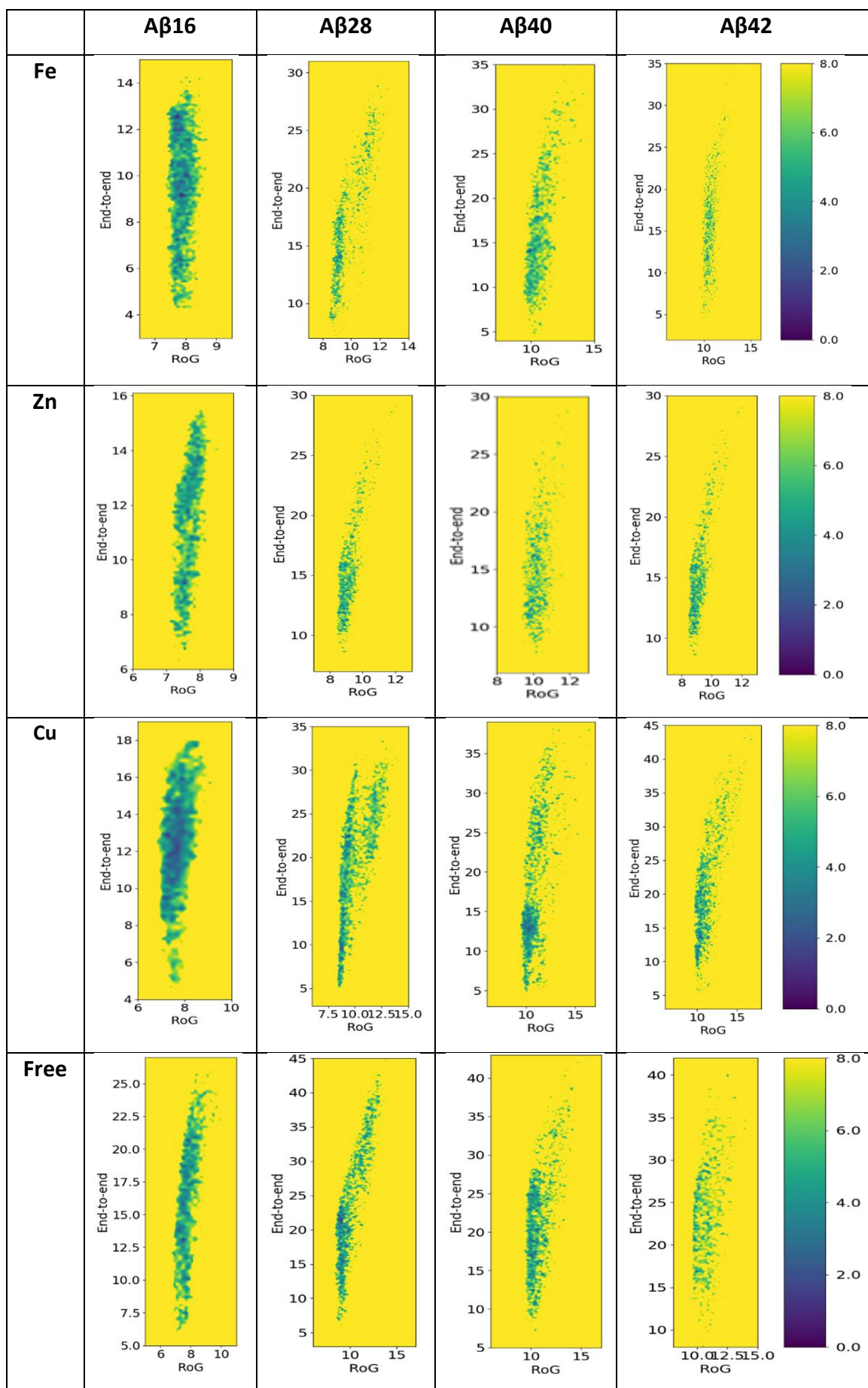
This is supported by RMSF data indicating an enhanced level of lability especially within residue Asp1 when not bound to a metal centre but also at relatively increased levels in Aβ-Cu peptides compared to other transition metals investigated.

Accelerated MD was chosen as a method for this study due to its enhanced conformational sampling required for intrinsically disordered peptides of this size. Compared to previous studies conducted within our group[82] we observed increased conformational sampling from the range of Rg values reported. The number of discrete minima structures displayed within the 2D free-energy plots shows the need for the boost potential provided via aMD, since conventional MD could be expected to get trapped in low energy minima. Subsequent reweighting was effective at further highlighting the comparisons between structures as a function of free energy when comparing Rg, hydrogen bonds and end-to-end distances. From this data we are provided another example of the comparative results between zinc/iron and copper/free peptide.

Conclusions

From the results presented here, clear patterns emerged for the similarities in dynamics between two pairs of structures. Zinc and iron-bound peptides showed characteristically similar salt-bridge interactions and secondary structure profiles to one another in addition to ranges of data values occupied for minima structures displayed within 2-dimensional free energy plots. Likewise, free peptides and structures bound to Cu(II) displayed comparable results for salt-bridge incidence plots and Rg statistics.

Free peptides were shown to be more mobile compared to metal bound ones due to the lack of anchoring effect on bound residues. RMSF data clearly shows the greatest contribution to this reduced movement is from residues Asp1 and His6, which are bound in all metal simulations, showed the highest level of mobility in the unbound Aβ when compared to all other residues. In addition to the Rg data for these metal-free structures, the free peptides showed the highest levels of helical secondary structure as chain length increased. Levels of helical and strand secondary structure were reduced within the N-terminus of all peptides when bound to metal ions, demonstrating the anchoring effect of

metal centres in this region. Effects of metal binding were also shown to have a global effect on secondary structure at areas of the peptide remote from those used for coordination.

Since the first proposal of the amyloid cascade hypothesis, it was discovered that metal ions play an important role in the aggregation and formation of characteristic Aβ deposits. Specifically, that due to the high affinity of the transition metals Fe(II), Cu(II) and Zn(II), these ions bind readily to the peptide which leads to an increase in production of reactive oxygen species[83]. These in turn encourage formation of intermolecular bonds between monomeric Aβ peptides hindering the ability to dispose of any Aβ which has been overproduced as well as leading to this influx of ROS[84]. Studies suggest Cu(II) competes with Zn(II) ions for similar binding sites of Aβ[85]. Zinc-Aβ complexes appear to aggregate more readily in comparison to these copper-containing metallopeptides yet at high enough concentrations the rate of aggregation for Aβ-Cu increases to similar levels.

All three metals were analysed having different binding interactions with Aβ to one another, though this does not appear to have caused the simulations to possess motions completely independent of each other. Zn(II) and Fe(II), for example, form 4 and 5-coordinate structures respectively but still produce results indicative of similar structures, motions and interactions being sampled over the course of the trajectories.

Accelerated MD proved to be an effective computational method for investigating and comparing the structure and dynamics of peptides of this nature, reporting better conformational sampling compared to conventional MD. Further work could include simulating other peptide structures, different metal centres, binding modes or revisiting mutant peptide structures simulated previously within the research group for further comparative studies.

Acknowledgements

Author Contributions

ODKB carried out simulations and initial analysis, and wrote initial drafts; NA carried out simulations and initial analysis; JAP designed the study, carried out analysis and wrote final drafts of manuscript.

Supporting Information

Plots of RMSD and Rg for individual trajectories, numerical data for salt bridge incidence, secondary structure plots for all simulations, and PMFs for a range of properties are reported in Supporting Information.

References

1   "What is Alzheimer's" | Alzheimer's Association, (accessed 1st October 2021). Retrieved from https://alz.org/alzheimers-dementia/what-is-alzheimers

2   G. McKhann, D. Drachman, M. Folstein, R. Katzman, D. Price and E. Stadlan. (1984) Clinical diagnosis of Alzheimer's disease, *Neurology*, 34, 939–944.

3   "How many people have dementia and what is the cost of dementia care?" | Dementia UK Report (2019), (accessed 1st October 2021). Retrieved from: https://www.alzheimers.org.uk/about-us/policy-and-influencing/dementia-scale-impact-numbers

4   B. Alies, H. Eury, C. Bijani, L. Rechignat, P. Faller and C. Hureau. (2011) pH-Dependent Cu(II) Coordination to Amyloid-β Peptide: Impact of Sequence Alterations, Including the H6R and D7N Familial Mutations, *Inorg. Chem.*, 50 (21), 11192–11201.

5   D. J. Selkoe. (2008) Soluble oligomers of the amyloid β-protein impair synaptic plasticity and behavior, *Behav. Brain Res.*, 192 (1), 106–113.

6   P. A. Adlard and A. I. Bush. (2018) Metals and Alzheimer's Disease: How Far Have We Come in the Clinic?, *J. Alzheimer's Dis.*, 62 (3), 1369–1379.

7   S. Wärmländer, A. Tiiman, A. Abelein, J. Luo, J. Jarvet, K. L. Söderberg, J. Danielsson

and A. Gräslund. (2013) Biophysical studies of the amyloid β-peptide: Interactions with metal ions and small molecules, *ChemBioChem*, 14, 1692–1704.

8   Y. W. Zhang, R. Thompson, H. Zhang and H. Xu. (2011) APP processing in Alzheimer's disease, *Mol. Brain*, 4 (3), 1-13

9   S. C. Drew, C. J. Noble, C. L. Masters, G. R. Hanson and K. J. Barnham. (2009) Pleomorphic copper coordination by alzheimer's disease amyloid-β peptide, *J. Am. Chem. Soc.*, 131 (3), 1195–1207.

10   B. Jiao, B. Tang, X. Liu, J. Xu, Y. Wang, L. Zhou, F. Zhang, X. Yan, Y. Zhou and L. Shen. (2014) Mutational analysis in early-onset familial Alzheimer's disease in Mainland China, *Neurobiol. Aging*, 35 (8), 1957.e1-1957.e6.

11   K. P. Kepp. (2017) Alzheimer's disease: How metal ions define β-amyloid function, *Coord. Chem. Rev.*, 351, 127–159.

12   T. Iwatsubo, A. Odaka, N. Suzuki, H. Mizusawa, N. Nukina and Y. Ihara. (1994) Visualization of Aβ42(43) and Aβ40 in senile plaques with end-specific Aβ monoclonals: Evidence that an initially deposited species is Aβ42(43), *Neuron*, 13 (1), 45–53

13   R. A. Stelzmann, H. N. Schnitzlein and F. R. Murtagh. (1995) An English translation of Alzheimer's 1907 Paper, "Uber eine eigenartige Erlranliung der Hirnrinde", *Clin. Anat.*, 8, 429–43.

14   E. D. Eanes and G. G. Glenner. (1968) X-Ray Diffraction Studies On Amyloid Filaments, *J. Histochem. Cytochem.*, 16 (11), 673–677.

15   C. L. Masters, G. Simms, N. A. Weinman, G. Multhaupt, B. L. Mcdonald and K. Beyreuthert. (1985) Amyloid plaque core protein in Alzheimer disease and Down syndrome, 82, 4245-4249

16   J. A. Hardy and G. A. Higgin. (1992) Alzheimer's Disease: The Amyloid Cascade Hypothesis, *Science*, 256 (5054), 184–185.

17   W. I. Rosenblum. (2014) Why Alzheimer trials fail: Removing soluble oligomeric beta amyloid is essential, inconsistent, and difficult, *Neurobiol. Aging*, 35 (5), 969–974.

18   W. L. Klein. (2002) Aβ toxicity in Alzheimer's disease: Globular oligomers (ADDLs) as new vaccine and drug targets, *Neurochem. Int.*, 41 (5), 345–352.

19   R. Ricciarelli and E. Fedele. (2017) Aβ toxicity in Alzheimer's disease: Globular oligomers (ADDLs) as new vaccine and drug targets, *Curr. Neuropharmacol.*, 15 (6), 926–935.

20   A. I. Bush. (2003) The metallobiology of Alzheimer's disease*, Trends Neurosci.*, 26 (4), 207–214.

21   M. A. Lovell, J. D. Robertson, W. J. Teesdale, J. L. Campbell and W. R. Markesbery. (1998) Copper, iron and zinc in Alzheimer's disease senile plaques, *J. Neurol. Sci.*, 158 (1), 47–52.

22   S. Boopathi, P. Dinh Quoc Huy, W. Gonzalez, P. E. Theodorakis and M. S. L. (2020) Zinc binding promotes greater hydrophobicity in Alzheimer's Aβ42 peptide than copper binding: Molecular dynamics and solvation thermodynamics studies, *Proteins Struct. Funct. Bioinf.*, 88 (10), 1285–1302.

23   C. Ballard, S. Gauthier, A. Corbett, C. Brayne, D. Aarsland and E. Jones.(2011) Alzheimer's disease, *Lancet*, 377, 1019–1031.

24   J. Hardy. (2006) Has the Amyloid Cascade Hypothesis for Alzheimers Disease been Proved?, *Curr. Alzheimer Res.*, 3 (1), 71–73.

25   W. T. Chen, C. J. Hong, Y. T. Lin, W. H. Chang, H. T. Huang, J. Y. Liao, Y. J. Chang, Y. F. Hsieh, C. Y. Cheng, H. C. Liu, Y. R. Chen and I. H. Cheng. (2012) Amyloid-beta (Aβ) D7H mutation increases oligomeric Aβ42 and alters properties of Aβ-zinc/copper assemblies, *PLoS One*, 7 (4), e35807

26   K. Halverson, P. E. Fraser, D. A. Kirschner and P. T. Lansbury. (1990) Molecular Determinants of Amyloid Deposition in Alzheimer's Disease: Conformational Studies of Synthetic β-Protein Fragments, *Biochemistry*, 29 (11), 2639–2644.

27   L. K. Simmons, P. C. May, K. J. Tomaselli, R. E. Rydel, K. S. Fuson, E. F. Brigham, S. Wright, I. Lieberburg, G. W. Becker and D. N. Brems. (1994) Secondary structure of amyloid beta peptide correlates with neurotoxic activity in vitro, *Mol. Pharmacol.*, 45

(3), 373–9.

28   A. Lomakin, D. Soo Chung, G. B. Benedek, D. A. Kirschner and D. B. Teplow. (1996) On
        the nucleation and growth of amyloid ,8-protein fibrils: Detection of nuclei and
        quantitation of rate constants (Alzheimer disease/fibrillogenesis/light scattering),
        Biophysics, 93, 1125-1129

29   T. T. M. Thu, N. T. Co, L. A. Tu and M. S. Li. (2019) Aggregation rate of amyloid beta
        peptide is controlled by beta-content in monomeric state, *J. Chem. Phys.*, 150 (22),
        225101.

30   J. A. Duce and A. I. Bush. (2010) Biological metals and Alzheimer's disease:
        Implications for therapeutics and diagnostics, *Prog. Neurobiol.*, 92 (1), 1–18.

31   V. Balland, C. Hureau and J.-M. Savéant. (2010) Electrochemical and homogeneous
        electron transfers to the Alzheimer amyloid-β copper complex follow a
        preorganization mechanism, PNAS, 5 (40), 17113–17118.

32   V. Minicozzi, F. Stellato, M. Comai, M. Dalla Serra, C. Potrich, W. Meyer-Klaucke and
        S. Morante. (2008) Identifying the minimal copper- and zinc-binding site sequence in
        amyloid-β peptides, *J. Biol. Chem.*, 283 (16), 10784–10792.

33   Y. H. Hung, A. I. Bush and R. A. Cherny. (2010) Copper in the brain and Alzheimer's
        disease, *J. Biol. Inorg. Chem.*, 15 (1), 61–76.

34   A. I. Bush and R. E. Tanzi. (2008) Therapeutics for Alzheimer's Disease Based on the
        Metal Hypothesis, *Neurotherapeutics*, 5 (3), 421-431

35   P. R. L. Markwick and J. A. McCammon. (2011) Studying functional dynamics in bio-
        molecules using accelerated molecular dynamics, *Phys. Chem. Chem. Phys.*, 13 (45),
        20053–20065.

36   A. Okur, L. Wickstrom, M. Layten, R. Geney, K. Song, V. Hornak and C. Simmerling.
        (2006) Improved efficiency of replica exchange simulations through use of a hybrid
        explicit/implicit solvation model, *J. Chem. Theory Comput.*, 2 (2), 420–433.

37   R. Geney, M. Layten, R. Gomperts, V. Hornak and C. Simmerling, (2006) Investigation
        of salt bridge stability in a generalized born solvent model, *J. Chem. Theory Comput.*,

2 (1), 115–127.

38   D. Hamelberg, J. Mongan and J. A. McCammon. (2004) Accelerated molecular dynamics: A promising and efficient simulation method for biomolecules, *J. Chem. Phys.*, 120 (24), 11919–11929.

39   J. Talafous, K. J. Marcinowski, G. Klopman and M. G. Zagorski. (1994) Solution Structure of Residues 1–28 of the Amyloid β-Peptide, *Biochemistry*, 33 (25), 7788–7796.

40   K. Kirshenbaum and V. Daggett. (1995) pH-Dependent Conformations of the Amyloid β(1-28) Peptide Fragment Explored Using Molecular Dynamics, *Biochemistry*, 34 (23), 7629–7639.

41   T. Kowalik-Jankowska, M. Ruta, K. Wisniewska and L. Lankiewicz. (2003) Coordination abilities of the 1–16 and 1–28 fragments of b-amyloid peptide towards copper(II) ions: a combined potentiometric and spectroscopic study, *J. Inorg. Biochem.*, 95, 270–282.

42   N. Ntarakas, I. Ermilova and A. P. Lyubartsev. (2019) Effect of lipid saturation on amyloid-beta peptide partitioning and aggregation in neuronal membranes: molecular dynamics simulations, *Eur. Biophys. J.*, 48 (8), 813–824.

43   *Molecular Operating Environment (MOE),* (2013) 1010 Sherbrooke St. West, Suite #910, Chemical Computing Group ULC, Montreal, QC, Canada, H3A 2R7

44   E. Atrián-Blasco, M. Del Barrio, P. Faller and C. Hureau. (2018) Ascorbate Oxidation by Cu(Amyloid-β) Complexes: Determination of the Intrinsic Rate as a Function of Alterations in the Peptide Sequence Revealing Key Residues for Reactive Oxygen Species Production, *Anal. Chem.*, 90 (9), 5909–5915.

45   F. Bousejra-Elgarah, C. Bijani, Y. Coppel, P. Faller and C. Hureau. (2011) Iron(II) binding to amyloid-β, the Alzheimer's peptide, *Inorg. Chem.*, 50 (18), 9024–9030.

46   J. Nasica-Labouze, P. H. Nguyen, F. Sterpone, O. Berthoumieu, N. V. Buchete, S. Coté, A. De Simone, A. J. Doig, P. Faller, A. Garcia, A. Laio, M. S. Li, S. Melchionna, N. Mousseau, Y. Mu, A. Paravastu, S. Pasquali, D. J. Rosenman, B. Strodel, B. Tarus, J. H.

Viles, T. Zhang, C. Wang and P. Derreumaux. (2015) Amyloid β Protein and Alzheimer's Disease: When Computer Simulations Complement Experimental Studies, *Chem. Rev.*, 115 (9), 3518–3563.

47   H. Kozlowski, M. Luczkowski, M. Remelli and D. Valensin. (2012) Copper, zinc and iron in neurodegenerative diseases (Alzheimer's, Parkinson's and prion diseases), *Coord. Chem. Rev.*, 256 (19-20), 2129–2141.

48   W. D. Cornell, P. Cieplak, C. I. Bayly, I. R. Gould, K. M. Merz, D. M. Ferguson, D. C. Spellmeyer, T. Fox, J. W. Caldwell and P. A. Kollman. (1995) A Second Generation Force Field for the Simulation of Proteins, Nucleic Acids, and Organic Molecules, *J. Am. Chem. Soc.*, 117 (19), 5179–5197.

49   R. J. Deeth, N. Fey and B. Williams-Hubbard. (2005) DommiMOE: An implementation of ligand field molecular mechanics in the molecular operating environment, *J. Comput. Chem.*, 26 (2), 123–130.

50   D.A. Case, R.M. Betz, D.S. Cerutti, T.E. Cheatham, III, T.A. Darden, R.E. Duke, T.J. Giese, H. Gohlke, A.W. Goetz, N. Homeyer, S. Izadi, P. Janowski, J. Kaus, A. Kovalenko, T.S. Lee, S. LeGrand, P. Li, C. Lin, T. Luchko, R. Luo, B. Madej, D. Mermelstein, K.M. Merz, G. Monard, H. Nguyen, H.T. Nguyen, I. Omelyan, A. Onufriev, D.R. Roe, A. Roitberg, C. Sagui, C.L. Simmerling, W.M. Botello-Smith, J. Swails, R.C. Walker, J. Wang, R.M. Wolf, X. Wu, L. Xiao and P.A. Kollman. (2016), AMBER 2016, University of California, San Francisco.

51   J. A. Maier, C. Martinez, K. Kasavajhala, L. Wickstrom, K. E. Hauser and C. Simmerling. (2015) ff14SB: Improving the Accuracy of Protein Side Chain and Backbone Parameters from ff99SB, *J. Chem. Theory Comput.*, 11 (8), 3696–3713.

52   Zhang, W, Hou, T, Schafmeister, C, Ross, W. S, Case, D. A. (2010) LEaP and gleap: AmberTools Users' Manual Version 1.4,

53   P. Li and K. M. Merz. (2016) MCPB.py: A Python Based Metal Center Parameter Builder, *J. Chem. Inf. Model.*, 56 (4), 599–604.

54   M. J. Frisch, G. W. Trucks, H. B. Schlegel, G. E. Scuseria, M. A. Robb, J. R. Cheeseman, G. Scalmani, V. Barone, G. A. Petersson, H. Nakatsuji, X. Li, M. Caricato, A. Marenich,

J. Bloino, B. G. Janesko, R. Gomperts, B. Mennucci, H. P. Hratchian, J. V. Ortiz, A. F. Izmaylov, J. L. Sonnenberg, D. Williams-Young, F. Ding, F. Lipparini, F. Egidi, J. Goings, B. Peng, A. Petrone, T. Henderson, D. Ranasinghe, V. G. Zakrzewski, J. Gao, N. Rega, G. Zheng, W. Liang, M. Hada, M. Ehara, K. Toyota, R. Fukuda, J. Hasegawa, M. Ishida, T. Nakajima, Y. Honda, O. Kitao, H. Nakai, T. Vreven, K. Throssell, J. A. Montgomery, Jr., J. E. Peralta, F. Ogliaro, M. Bearpark, J. J. Heyd, E. Brothers, K. N. Kudin, V. N. Staroverov, T. Keith, R. Kobayashi, J. Normand, K. Raghavachari, A. Rendell, J. C. Burant, S. S. Iyengar, J. Tomasi, M. Cossi, J. M. Millam, M. Klene, C. Adamo, R. Cammi, J. W. Ochterski, R. L. Martin, K. Morokuma, O. Farkas, J. B. Foresman, and D. J. Fox. (2016) Gaussian, Inc., Wallingford CT

55   J. M. Seminario. (1996) Calculation of intramolecular force fields from second-derivative tensors, *Int. J. Quantum Chem.*, 60 (7), 1271–1277.

56   W. Clark Still, A. Tempczyk, R. C. Hawley and T. Hendrickson. (1990) Semianalytical Treatment of Solvation for Molecular Mechanics and Dynamics, *J. Am. Chem. Soc.*, 112, 6127–9.

57   R. Constanciel and R. Contreras. (1984) Self consistent field theory of solvent effects representation by continuum models: Introduction of desolvation contribution, *Theor. Chim. Acta*, 65 (1), 1–11.

58   M. Schaefer and M. Karplus. (1996) A comprehensive analytical treatment of continuum electrostatics, *J. Phys. Chem.*, 100 (5), 1578–1599.

59   N. Al-Shammari, L. Savva and O. Kennedy-Britten. (2021) Forcefield evaluation and accelerated molecular dynamics simulation of Zn(II) binding to N-terminus of amyloid-β, *Comput. Biol. Chem.,* 93, 107540

60   M. Cecchini, R. Curcio, M. Pappalardo, R. Melki and A. Caflisch. (2006) A molecular dynamics approach to the structural characterization of amyloid aggregation, *J. Mol. Biol.*, 357 (4), 1306–1321.

61   W. L. Jorgensen, J. Chandrasekhar, J. D. Madura, R. W. Impey and M. L. Klein. (1983) Comparison of simple potential functions for simulating liquid water, *J. Chem. Phys.*, 79 (2), 926–935.

62   A. V Onufriev and D. A. Case. (2019) Generalized Born Implicit Solvent Models for Biomolecules, *Annu. Rev. Biophys.*, 48, 275–296.

63   R. Anandakrishnan, A. Drozdetski, R. C. Walker and A. V. Onufriev. (2015) Speed of conformational change: Comparing explicit and implicit solvent molecular dynamics simulations, *Biophys. J.*, 108 (5), 1153–1164.

64   J. A. Izaguirre, D. P. Catarello, J. M. Wozniak and R. D. Skeel. (2001) Langevin stabilization of molecular dynamics, *J. Chem. Phys.*, 114 (5), 2090–2098.

65   S. V Lushchekina, E. D. Kots, D. A. Novichkova, K. A. Petrov and P. Masson. (2017) Role of Acetylcholinesterase in β-Amyloid Aggregation Studied by Accelerated Molecular Dynamics, *Bionanoscience*, 7 (2), 396–402.

66   B. Zhao, M. A. Cohen Stuart and C. K. Hall. (2017) Navigating in foldonia: Using accelerated molecular dynamics to explore stability, unfolding and self-healing of the β-solenoid structure formed by a silk-like polypeptide, *PLoS Comput. Biol.*, 13 (3), 1-22

67   J. P. Ryckaert, G. Ciccotti and H. J. C. Berendsen. (1977) Numerical integration of the cartesian equations of motion of a system with constraints: molecular dynamics of n-alkanes, *J. Comput. Phys.*, 23 (3), 327–341.

68   D. R. Roe and T. E. Cheatham. (2013) PTRAJ and CPPTRAJ: Software for processing and analysis of molecular dynamics trajectory data, *J. Chem. Theory Comput.*, 9 (7), 3084–3095.

69   W. Humphrey, A. Dalke and K. Schuten. (1996) VMD: Visual Molecular Dynamics, *J. Mol. Graphics*, 14, 33–38.

70   W. Sinko, Y. Miao, C. A. F. De Oliveira and J. A. McCammon. (2013) Population based reweighting of scaled molecular dynamics, *J. Phys. Chem. B*, 117 (42), 12759–12768.

71   Y. Miao, W. Sinko, L. Pierce, D. Bucher, R. C. Walker and J. A. McCammon. (2014) Improved reweighting of accelerated molecular dynamics simulations for free energy calculation, *J. Chem. Theory Comput.*, 10 (7), 2677–2689.

72   P. D. Q. Huy, Q. Van Vuong, G. La Penna, P. Faller and M. S. Li. (2016) Impact of Cu(II) Binding on Structures and Dynamics of Aβ42Monomer and Dimer: Molecular

Dynamics Study, *ACS Chem. Neurosci.*, 7 (10), 1348–1363.

73   M. Ester, H. P. Kriegel, S. J. and X. Xu. (1996) A density-based algorithm for discovering clusters in large spatial databases with noise, *Proc. 2nd Int. Conf. Knowl. Discov. Data Min.*, 7, 226–231.

74   B. Strodel and O. Coskuner-Weber. (2019) Transition Metal Ion Interactions with Disordered Amyloid-β Peptides in the Pathogenesis of Alzheimer's Disease: Insights from Computational Chemistry Studies, *J. Chem. Inf. Model.*, 59 (5), 1782–1805.

75   S. Vivekanandan, J. R. Brender, S. Y. Lee and A. Ramamoorthy. (2011) A partially folded structure of amyloid-beta(1-40) in an aqueous environment, *Biochem. Biophys. Res. Commun.*, 411 (2), 312–316.

76   A. Schmechel, H. Zentgraf, S. Scheuermann, G. Fritz, R. Pipkorn, J. Reed, K. Beyreuther, T. A. Bayer and G. Multhaup. (2003) Alzheimer β-amyloid homodimers facilitate Aβ fibrillization and the generation of conformational antibodies, *J. Biol. Chem.*, 278 (37), 35317–35324.

77   K. L. Sciarretta, D. J. Gordon, A. T. Petkova, R. Tycko and S. C. Meredith. (2005) Aβ40-lactam(D23/K28) models a conformation highly favorable for nucleation of amyloid, *Biochemistry*, 44 (16), 6003–6014.

78   S. T. Mutter, M. Turner, R. J. Deeth and J. A. Platts. (2018), Metal Binding to Amyloid-β 1–42 : A Ligand Field Molecular Dynamics Study, *ACS Chem. Neurosci.*, 9, 2795-2806.

79   X. Zheng, D. Liu, R. Roychaudhuri, D. B. Teplow and M. T. Bowers. (2015) Amyloid β-Protein Assembly: Differential Effects of the Protective A2T Mutation and Recessive A2V Familial Alzheimer's Disease Mutation, *ACS Chem. Neurosci.*, 6, 1732–1740.

80   C. Wurth, N. K. Guimard and M. H. Hecht. (2002) Mutations that reduce aggregation of the Alzheimer's Aβ42 peptide: An unbiased search for the sequence determinants of Aβ amyloidogenesis, *J. Mol. Biol.*, 319 (5), 1279–1290.

81   C. Talmard, L. Guilloreau, Y. Coppel, H. Mazarguil and P. Faller. (2007) Amyloid-beta peptide forms monomeric complexes with CuII and ZnII prior to aggregation,

ChemBioChem, 8 (2), 163–165.

82   O. D. Kennedy-Britten, N. Al-Shammari and J. A. Platts. (2020) Molecular dynamics simulations of copper binding to N-terminus mutants of amyloid-β, *J. Biomol. Struct. Dyn.*, 39 (6), 2003-2013

83   C. Cheignon, M. Jones, E. Atrián-Blasco, I. Kieffer, P. Faller, F. Collin and C. Hureau. (2017) Identification of key structural features of the elusive Cu-Aβ complex that generates ROS in Alzheimer's disease, *Chem. Sci.*, 8 (7), 5107–5118.

84   J. Alí-Torres, A. Mirats, J. D. Maréchal, L. Rodríguez-Santiago and M. Sodupe. (2014) 3D structures and redox potentials of Cu2+-Aβ(1-16) complexes at different pH: A computational study, *J. Phys. Chem. B*, 118 (18), 4840–4850.

85   K. Suzuki, T. Miura and H. Takeuchi. (2001) Inhibitory effect of copper(II) on zinc(II)-induced aggregation of amyloid β-peptide, *Biochem. Biophys. Res. Commun.*, 285 (4), 991–996.